

## Quantum transport on generalized scale-free networks

Cássio Macêdo Maciel,<sup>1</sup> Carlos F. O. Mendes <sup>1,2</sup> Walter T. Strunz,<sup>3</sup> and Mircea Galiceanu <sup>1,\*</sup>

<sup>1</sup>*Departamento de Física, Universidade Federal do Amazonas, 69077-000 Manaus, Brazil*

<sup>2</sup>*Escola Normal Superior, Universidade do Estado do Amazonas, 69050-010 Manaus, Brazil*

<sup>3</sup>*Institut für Theoretische Physik, Technische Universität Dresden, 01062 Dresden, Germany*



(Received 22 June 2020; accepted 2 September 2020; published 25 September 2020)

We consider quantum transport on generalized scale-free networks (GSFNs) in the continuous-time quantum walk (CTQW) model. The efficiency of the transport is monitored through the exact and the average return probabilities. In this model these probabilities are fully determined by the eigenvalues and eigenvectors of the connectivity matrix. In the case of GSFNs we observe a nontrivial interplay between strong localization effects, due to starlike segments, and good spreading because of the linear segments. We show that the quantum transport on GSFNs can be increased by varying the minimum or the maximum allowed degrees, i.e., the limiting number of links emerging from every node. The same quantum efficiency is reached by considering various combinations of the construction parameters of the network, which normally show different topological features.

DOI: [10.1103/PhysRevA.102.032219](https://doi.org/10.1103/PhysRevA.102.032219)

### I. INTRODUCTION

Classical and quantum transport have been applied with great success to many processes from physics, chemistry, biology, and computer science. Classical random walks (RWs) in different kinds of complex systems have been studied in recent decades [1–7]. The concept of the RW was implemented to solve problems related to configurational properties of polymers [8], kinetic chemical reactions [2,9,10], diffusion of particles or complex systems [11–13], and epidemic spreading of diseases or viruses [14,15], to name only a few. However, some phenomena are better understood by considering the quantum mechanical variant of RWs: quantum walks (QWs).

Quantum walks can model purely coherent quantum dynamics of excitations on complex systems [16–25]. QWs are closely related to quantum graphs [26–31], which additionally take into account the inherited properties of each bond: in quantum graphs the bonds may be directed, have distinct coupling strength, or have different lengths. An application based on quantum walks is the quantum search algorithm for quantum computation [32–39]. The most prominent examples are Grover’s search algorithm [40] and Shor’s algorithm [41]. These algorithms search for an unstructured database of qubits and they improve polynomially and even exponentially the speedup, compared to the corresponding classical algorithms. Quantum spatial search algorithms have been implemented also for complex lattices, such as  $d$ -dimensional square lattices [42] and graphene lattices [43]. The consistent increase of the speedup has also started an avalanche of experimental works [33,34,44–66].

The walkers’ dynamics can be studied by making use of one of two distinct models: the discrete-time model and

the continuous-time model. The same holds true in quantum transport [67,68], where we have the discrete-time quantum walk (DTQW) [69] and the continuous-time quantum walk (CTQW) [70]. However, these two models are not completely independent; they can be related to each other as shown in [71]. In the literature one encounters alternatives for these models, such as the quantum stochastic walk [72–74] and a Green’s function approach for quantum graphs [75,76]. Here, we focus on the CTQW model, which solves the dynamics of the quantum walk by identifying the Hamiltonian with the transfer matrix. Similarly to the classical case in the CTQW model, the transfer matrix of any undirected network is associated with the connectivity matrix [1]. In this model the quantum transport is practically solved when one knows the full eigenvalue spectrum of the connectivity matrix. In this article the efficiency of the walkers’ dynamics (or search) is evaluated by the probability of returning to its starting node.

Nowadays, the concept of complex networks is applied to many scientific studies related to various research areas, such as physics, chemistry, biology, sociology, ecology, economic systems, and computer science; see [77–79] and references therein. The vast majority of these applications can be studied through three well-established theoretical models, namely the random network, small-world network, and scale-free network. We focus on the last type due to the fact that many real networks are scale-free networks. More precisely, we concentrate on the most important property of this type of network, namely the existence of *hubs*, i.e., nodes with a high number of connections, and many nodes with few connections. Thus, we are led to a degree distribution that follows a power law [80,81]. Here, we add some restrictions to the degree distribution, such as the minimum and the maximum allowed number of links [82]. These conditions can be justified by spatial limitations around each nodes or by some sort of weaker or stronger interaction strength between nodes.

\*mircea@ufam.edu.br

We are mainly interested in monitoring the influence of the above-mentioned parameters on quantum transport on generalized scale-free networks. It is known that we have a strong relation between the transport and the underlying structure of the network. The quantum transport on graphs that contain segments with many branches, such as Cayley trees or stars [83,84], displays strong localization effects, i.e., high probability to stay at the initial node. A completely distinct behavior is found for linear chains, which have a high efficiency for quantum transport, as shown in the literature [83]. Our generalized scale-free networks are a nontrivial mixture of linear and starlike segments, with their topology being controlled by the minimum and maximum allowed degrees and by the exponent  $\gamma$  of the power-law degree distribution. This last parameter allows us to switch from networks with a predominant starlike topology, for low values of  $\gamma$ , to networks with longer linear chains, for high  $\gamma$  values. Our main focus is to improve the quantum transport and to overcome the localization problem encountered in networks with starlike segments. We have shown that a possible solution is to implement some mechanisms to increase the length of linear segments. This can be done by stacking identical copies on top of each other [85], creating a multilayer network. Another mechanism could be an internal increase of linear segments by adding links between nodes from a given structure in a certain manner [86]. Another possible mechanism to increase the transfer efficiency is given by introducing noise or decoherence in the network [87,88]. Here, we choose another mechanism to increase the quantum transport: restrict the minimum and the maximum allowed degrees of a certain type of network.

The paper is organized as follows. In Sec. II we focus on a general description of the continuous-time classical and quantum models implemented in the paper. In Sec. III we describe the construction procedure of our networks. Section IV is devoted to the results, focusing on the eigenvalue spectrum of the Laplacian matrix and on physical quantities used to compute the classical and quantum transport in such networks. Finally in Sec. V we present our conclusions.

## II. THEORETICAL FRAMEWORK

In this article we are interested in quantum transport on generalized scale-free networks (GSFNs) using the continuous-time quantum walk (CTQW) model. For reasons of comparison, we also study the corresponding classical model, continuous-time random walks (CTRWs). We understand a network to be a set of  $N$  nodes that are connected to other nodes by links. In this formalism a state  $|k\rangle$  is associated with each node and it corresponds to an excitation localized at node  $k$ . The dynamics of a network, for continuous-time models, depends only on the direct links between the nodes. This localization of the walks can be completely found out if one knows the whole set of eigenvalues and eigenvectors of the connectivity matrix  $\mathbf{A}$ . This  $N \times N$  matrix is real and symmetric, having its nondiagonal elements  $A_{jk}$  equal to  $-1$  if nodes  $i$  and  $j$  are linked, and  $0$  otherwise. The diagonal elements  $A_{jj} = k_j$  equal the number of links emerging from node  $j$ . From this matrix construction we inherit only positive real eigenvalues and a single vanishing eigenvalue,  $\lambda_1 = 0$ .

In classical transport we consider for simplicity an equal transition rate between neighbor nodes, chosen to be equal to 1. Assuming a Markovian process we obtain the following master equation for a CTRW to go from node  $k$  to node  $j$  at time  $t$  [2]:

$$\frac{d}{dt}p_{j,k}(t) = \sum_l T_{jl}p_{l,k}(t), \quad (1)$$

where  $T_{jl}$  is the transition rate between nodes  $j$  and  $l$ . In our model this transfer matrix is proportional to the connectivity matrix,  $\mathbf{T} = -\mathbf{A}$ . Thus, the transition probability of CTRWs depends on the eigenvalues  $\lambda_n$  and the eigenstates  $|\Phi_n\rangle$  (with  $n = 1, \dots, N$ ) of the connectivity matrix:

$$p_{j,k}(t) = \sum_{n=1}^N e^{-\lambda_n t} \langle j|\Phi_n\rangle \langle \Phi_n|k\rangle. \quad (2)$$

For quantum transport we assume that all the states  $|j\rangle$  are orthonormal and complete [70,83]. The dynamics of the walker is determined from the quantum mechanical Hamiltonian, such that Schrödinger's equation for the transition amplitudes  $\alpha_{j,k}(t) = \langle j|\exp(-i\mathbf{H}t)|k\rangle$  is

$$\frac{d}{dt}\alpha_{j,k}(t) = -i \sum_l H_{jl}\alpha_{l,k}(t). \quad (3)$$

Similarly to the CTRW, the quantum transition probability from node  $k$  to node  $j$  at time  $t$  is  $\pi_{j,k}(t) = |\alpha_{j,k}(t)|^2 = |\langle j|\exp(-i\mathbf{H}t)|k\rangle|^2$ . In this model the Hamiltonian is identified with the connectivity matrix [70]:  $\mathbf{H} = \mathbf{A}$ . Denoting the eigenstates of  $\mathbf{H}$  by  $|\Psi_n\rangle$ , and the quantum mechanical transition probability is

$$\pi_{j,k}(t) = \left| \sum_{n=1}^N e^{-i\lambda_n t} \langle j|\Psi_n\rangle \langle \Psi_n|k\rangle \right|^2. \quad (4)$$

Here we focus on the transport efficiency, and we determine the average return probabilities and the long-time average. The probability to remain or return to the initial node  $k$  is averaged over all nodes:

$$p(t) = \frac{1}{N} \sum_{k=1}^N p_{k,k}(t) \quad (5)$$

for CTRWs and

$$\bar{\pi}(t) = \frac{1}{N} \sum_{k=1}^N \pi_{k,k}(t) \quad (6)$$

for CTQWs. For CTRWs we insert Eq. (2) into Eq. (5) and we obtain that the average return probability depends exclusively on the eigenvalues of the connectivity matrix:

$$p(t) = \frac{1}{N} \sum_{k=1}^N \exp(-\lambda_k t). \quad (7)$$

For CTQWs we insert Eq. (4) into Eq. (6) and after some mathematical manipulations we find that the average return probability depends also on the eigenstates. However, by making use of the Cauchy-Schwarz inequality one gets a lower

bound for  $\bar{\pi}(t)$ , which is independent of the eigenstates:

$$\begin{aligned} \bar{\pi}(t) &= \frac{1}{N} \sum_{k=1}^N |\alpha_{k,k}(t)|^2 \geq \left| \frac{1}{N} \sum_{k=1}^N \alpha_{k,k}(t) \right|^2 \\ &= |\bar{\alpha}(t)|^2 = \left| \frac{1}{N} \sum_k \exp(-i\lambda_k t) \right|^2. \end{aligned} \quad (8)$$

However, in this paper we focus on the average return probabilities,  $p(t)$ , given by Eq. (7), and  $\bar{\pi}(t)$ , given by Eqs. (6) and (4). At this point we stress that a fast decay of  $p(t)$  or  $\bar{\pi}(t)$  implies a fast spreading of the walker and a slow decay implies a slow propagation throughout the structure. In the long-time limit one gets from Eq. (7) the equipartition value  $1/N$  for CTRWs, while for CTQWs both  $\bar{\pi}(t)$  and  $|\bar{\alpha}(t)|^2$  do not reach a constant value, but they present an oscillatory behavior around the long-time average value, given by [83]

$$\chi \equiv \lim_{t \rightarrow \infty} \frac{1}{t} \int_0^t dt' |\bar{\alpha}(t')|^2 \leq \lim_{t \rightarrow \infty} \frac{1}{t} \int_0^t dt' \bar{\pi}(t') \equiv \bar{\chi}, \quad (9)$$

where the Cauchy-Schwarz inequality, Eq. (8), was used. The average transition probability  $|\bar{\alpha}(t)|^2$  depends only on the eigenvalue density  $\rho(\lambda)$  of the connectivity matrix  $\mathbf{A}$  as [89]  $|\bar{\alpha}(t)|^2 = \sum_{\lambda, \lambda'} \rho(\lambda)\rho(\lambda') \exp[i(\lambda - \lambda')t]$ . Inserting the last equation in  $\bar{\chi}$  and identifying the integral with  $\delta_{\lambda\lambda'}$ , the long-time average transition probability can be written as [89,90]

$$\chi = \sum_{\lambda} \rho^2(\lambda) \geq \rho^2(\lambda^*) + \frac{1}{N} [1 - \rho(\lambda^*)] \equiv \chi^*, \quad (10)$$

where  $\lambda^*$  is the most degenerate eigenvalue. The quantum transport has maximum efficiency if  $\chi = 0$  and it is completely inefficient when  $\chi = 1$ . Regarding  $\chi^*$ , it was observed that it provides a good approximation for stars and linear chains [89]. For a star with  $N - 1$  arms we have a single highly degenerate eigenvalue  $\lambda^* = 1$  and it can be shown that  $\chi = \chi^* = [2 + (N - 2)^2]/N^2$ . In the limit of very large structures,  $\chi_{N \rightarrow \infty} = 1$ , which corresponds to an inefficient transport. For a linear chain all the eigenvalues are nondegenerate, which means that  $\rho(\lambda) = 1/N$  for every  $\lambda$ , yielding  $\chi = \chi^* = 1/N$ . In the limit of extremely long chains we have an efficient transport,  $\chi_{N \rightarrow \infty} = 0$ . In other situations the value of  $\chi^*$  does not provide a good approximation for  $\chi$ , as we show for different structures [85,86].

### III. GENERALIZED SCALE-FREE NETWORKS

Any complex network is represented by a collection of nodes connected by links. For each node one can determine the degree  $k$ , which is defined as the number of links emerging from the node. A basic property of all scale-free models [80,81,91–93] is a power-law decay for the degree distribution, i.e., the probability of having a node with degree  $k$  is  $\bar{p}_k \propto k^{-\gamma}$ , where the positive nonzero parameter  $\gamma$  measures the density of connections in the network. In this article we construct the treelike scale-free networks by assuming the probability  $p_k$ , that the degree of a node equals  $k$ , obeys the

following equation:

$$p_k = \begin{cases} \frac{k^{-\gamma}}{\sum_{j=K_{\min}}^{K_{\max}} j^{-\gamma}}, & K_{\min} \leq k \leq K_{\max}, \\ 0, & \text{otherwise,} \end{cases} \quad (11)$$

where  $K_{\min}$  is the minimum allowed degree and  $K_{\max}$  is the maximum allowed degree. The sum in the denominator keeps the sum of all probabilities equal to 1. The topology of our scale-free networks can be controlled by the three parameters  $\gamma$ ,  $K_{\min}$ , and  $K_{\max}$ , and it ranges from a pure linear network to a starlike network. Our model is the more general variant of the scale-free model developed in Ref. [81], which considers only  $(K_{\min}, K_{\max}) = (2, N - 1)$ , where  $N$  is the size of the network. For this reason we call our networks *generalized scale-free networks* (GSFNs) from now on. The construction procedure starts by fixing the three parameters mentioned above and the probabilities  $p_k$  are determined by implementing Eq. (11). We create the treelike networks by using a growth mechanism with the node degree being chosen from the distribution (11). When the construction ends the nodes will follow the degree distribution (11) with the exception of the peripheral nodes.

For a better understanding of the procedure we illustrate the algorithm for a particular realization with  $\gamma = 2.5$ ,  $K_{\min} = 2$ , and  $K_{\max} = 99$  in Fig. 1(d). In this figure the numbering was done according to the chronological order in which the nodes were built. We start by adding the first node, 1, whose degree is chosen at random from the degree distribution (11). For this particular network its chosen degree equals 15, meaning that we have to add fifteen new nodes connected to 1. In the next step we choose at random one of the open nodes and we select randomly its degree from the degree distribution (11). For the network of Fig. 1(d) the chosen node was 16 and its degree 4. Now we should add only three new nodes since node 16 already has one link with node 1. This procedure is iterated until we reach the total number of nodes,  $N$ . At this point the growth is finished and we assign to all remaining open nodes the degree 1.

In Fig. 1 we display several particular realizations of the algorithm for GSFNs with  $N = 100$  nodes. The parameter  $\gamma$  is equal to 1.0 in the first row, panels (a)–(c), and 2.5 in the last two rows, panels (d)–(i). In order to visualize the influence of parameter  $K_{\min}$  on the topology of the networks we choose for each column a different value of  $K_{\min}$ , namely 2, 3, and 6, from left to right. For a better visualization of some structural aspects we depicted by red thicker line the longest linear path, while the nodes with degree higher than 6 are drawn by larger circles. In order to see the treelike nature of these networks and to quickly compute the length of the longest path we drew the central node as a red color square and nodes with the same distance to the center share the same color. Full circles denote nodes that during the construction procedure have received their degree from Eq. (11). As a general rule one gets networks with higher longest linear path and with a lower number of hubs, i.e., nodes with very high degree, when only the parameter  $\gamma$  is increased. For instance by considering Fig. 1(a) ( $\gamma = 1.0$ ) and Fig. 1(d) ( $\gamma = 2.5$ ) one obtains the longest linear paths equal to 4 and 11, respectively. By fixing the parameters  $\gamma$  and  $K_{\max}$  and increasing the minimum allowed degree  $K_{\min}$  we usually increase the number

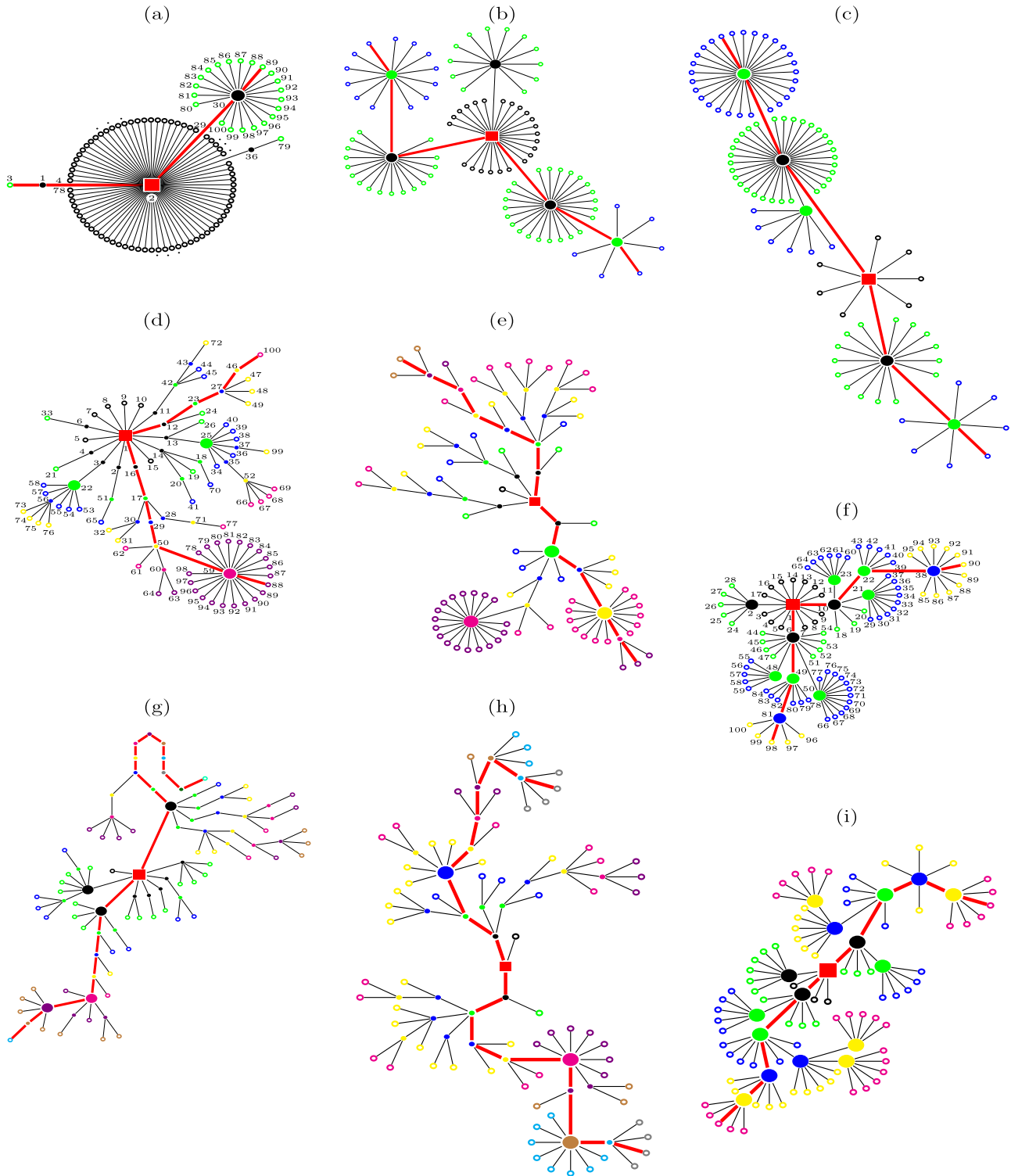


FIG. 1. Realizations of generalized scale-free networks with  $N = 100$  nodes and the parameter set  $(\gamma, K_{\min}, K_{\max})$ : (a) (1,2,99); (b) (1,3,99); (c) (1,6,99); (d) (2.5,2,99); (e) (2.5,3,99); (f) (2.5,6,99); (g) (2.5,2,10); (h) (2.5,3,10); (i) (2.5,6,10).

of nodes with higher degree. In this case the length of the longest linear path depends on all three parameters. One can find the same length by fine tuning these three parameters, for instance in both panels (b) and (c) of Fig. 1 the longest linear path equals 6. For more details regarding this issue one can follow Fig. 3 of Ref. [82], which focuses on the diameter of such networks, a quantity directly related to the longest linear

path. One way of increasing the longest linear segment is to reduce the maximum allowed degree  $K_{\max}$ , while the other two parameters are kept constant. This feature can be observed also by direct comparison of panels (d) and (g) of Fig. 1. At the same time we notice that the number of nodes with degree higher than 6 increases when  $K_{\max}$  gets lower, but fewer nodes have very high degree.

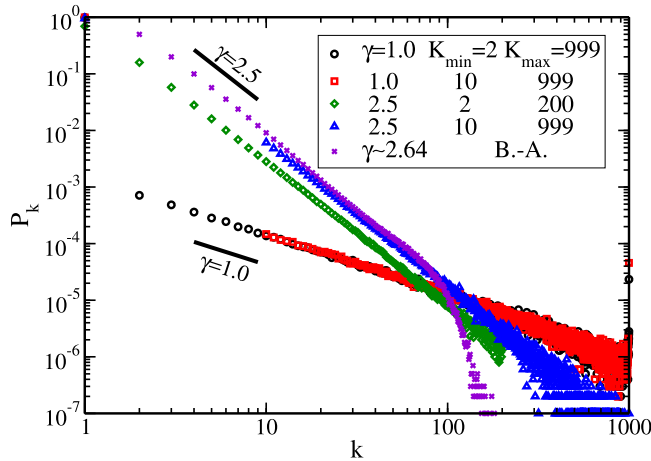


FIG. 2. Degree distribution  $p_k$  for GSFNs with  $N = 1000$ ,  $S = 10\,000$ , and various values of  $\gamma$ ,  $K_{\min}$ ,  $K_{\max}$ . For comparison we show the results for the Barabási-Albert model [80].

## IV. RESULTS

### A. Degree distribution

In Fig. 2 we display in double logarithmic scale the degree distribution  $p_k$  obtained from our constructed networks, which can be directly compared with the theoretical prediction, Eq. (11). Here we show the results for  $S = 10\,000$  realizations of the algorithm with the same network size,  $N = 1000$  nodes, with  $\gamma = 1.0$  and  $2.5$ , and various values of  $K_{\min}$  and  $K_{\max}$ . We also display the degree distribution of the Barabási-Albert model [80] for the same parameter set ( $N, S$ ) and for which we computed a power-law exponent  $\gamma \approx 2.64$ . For low and intermediate values of the degree  $k$  we recover the theoretically predicted values, with slopes of  $1.0$  or  $2.5$ , while for very high values of  $k$  we obtain the common *fat tail* behavior [80]. This means that usually we obtain networks with few nodes with very high degree and many nodes with low degrees. The rate between them is controlled by the power-law exponent. We get  $p_k = 0$  for  $k < K_{\min}$  and  $k > K_{\max}$ , except for  $p_1$ , which corresponds to peripheral nodes of our treelike scale-free networks, namely the nodes which did not receive their degree before finishing the construction. All these facts will have a big impact on the eigenvalue spectrum and on the classical and quantum transport.

### B. Eigenvalue spectra

In Fig. 3 we plot in double logarithmic scale the eigenvalue spectrum of GSFNs with  $(N, S) = (1000, 1000)$  and different values of the parameters  $\gamma$ ,  $K_{\min}$ , and  $K_{\max}$ . In Fig. 3(a) we keep constant the parameter set  $(K_{\min}, K_{\max})$  and we vary  $\gamma$ . Thus, we are able to monitor how the topology of the networks influences the eigenvalue spectrum. Immediately apparent is the multiplicity of the eigenvalue 1, which is proportional to the starlike predominance of the network. For reasons of comparison we display the spectrum for two limiting cases: a star with  $N - 1$  arms and a linear chain. The star has only three eigenvalues, namely  $\lambda_1 = 0$ ,  $\lambda_N = N$ , and  $\lambda_2 = \dots = \lambda_{N-1} = 1$ . In the case of a single linear chain all  $N$  eigenvalues are nondegenerate, with values between 0 and 4. In the case of

GSFNs the degeneracy of eigenvalue 1 is higher for low values of  $\gamma$ , due to an increase in the number of starlike segments, and it is lower for high  $\gamma$ s, namely networks with predominant linear topology. The lowest and the highest eigenvalues decrease when  $\gamma$  gets higher, having their minima when we have a complete linear chain.

In Fig. 3(b) we monitor the influence of the minimum allowed degree,  $K_{\min}$ , on the eigenvalue spectrum. Here we show the results for GSFNs with  $\gamma = 2.5$ , but similar findings are encountered for other values of  $\gamma$  and  $K_{\max}$ . The lowest and the highest eigenvalues increase when  $K_{\min}$  gets larger, which corresponds to networks composed of larger stars. We also can state that higher value of  $K_{\min}$  brings forth networks with higher degeneracy of the eigenvalue 1.

In Fig. 3(c) we plot the eigenvalues in progressive order for GSFNs with variable  $K_{\max}$  and fixed  $\gamma$  and  $K_{\min}$ . One can easily notice that even big changes of  $K_{\max}$  are less sensitive to the eigenvalue spectrum. Networks with intermediate and high  $\gamma$ , say,  $\gamma > 1$ , are predominantly formed by nodes with low degree, as can be seen also in Fig. 2. Thus, there are a few nodes which are altered when  $K_{\max}$  is diminished. The dependence on  $K_{\max}$  becomes more visible when  $\gamma$  is very low. In general, by decreasing  $K_{\max}$  the lowest nonvanishing eigenvalues and the highest eigenvalue are diminishing, which suggests an increase of the linearlike segments and a decrease in the number of branches. The last statement is strengthened by the degeneracy of eigenvalue 1, which is lower when  $K_{\max}$  is smaller.

In Fig. 3(d) we display a comparison between the eigenvalue spectrum of our GSFNs and the scale-free networks created from the Barabási-Albert model (B.-A.) [80]. In this model one starts with  $m_0$  vertices, chosen to be 3 in this figure, connected to each other. At each construction step we add a new node, which will be linked to two previously created vertices following a preferential attachment rule [80]. The construction stops when we have reached a total of  $N$  vertices. These scale-free networks follow a power-law degree distribution with exponent  $\gamma \approx 2.6$  and they are composed of loops, different from our GSFNs, which are trees. This aspect is responsible for the differences between the eigenvalue spectra of the models and it will have great consequences for classical and quantum transport. The presence of loops increases the total number of links and the net value of all eigenvalues increases. In general a compact network with  $m$  links between nodes has the eigenvalues' sum equal to  $2m$ . Thus, for a treelike network, like our GSFNs, the sum of all eigenvalues is  $2(N - 1)$ , while for the B.-A. networks we have  $4N - 6$ . In Fig. 3(d) we display the results for networks with  $N = 100, 500$ , and  $1000$ . For a better understanding of the results we choose  $\gamma = 2.6$  for GSFNs and we normalize the  $x$  axis to the size of the networks,  $N$ . We notice that the lower eigenvalues are very different, but the higher eigenvalues are comparable. The degeneracy of eigenvalue 1 practically disappears for B.-A., while for GSFNs it maintains a high number.

### C. Classical transport

In this section we study the classical transport in GSFNs. In Fig. 4(a) we investigate the influence of  $\gamma$ , i.e., the topology of the GSFN, on the probability of a walker returning

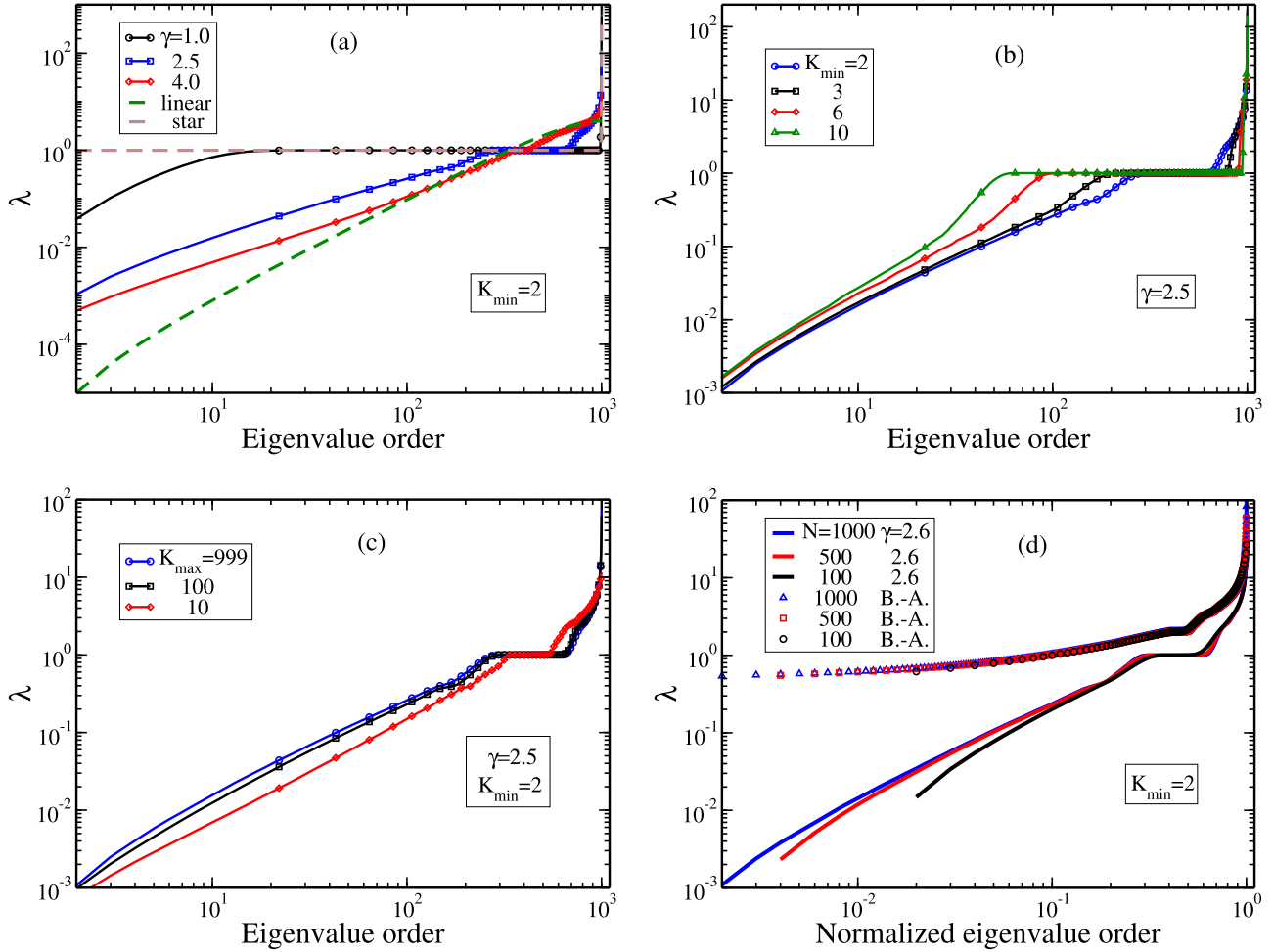


FIG. 3. Eigenvalue spectrum for GSFNs with  $N = 1000$ ,  $S = 1000$  and the parameters  $(\gamma, K_{\min}, K_{\max})$  are equal to (a) (variable, 2, 999), (b) (2.5, variable, 999), and (c) (2.5, 2, variable). In (d)  $N$  and  $S$  are varied and  $\gamma = 2.6$ ,  $K_{\min} = 2$ , and  $K_{\max} = N - 1$ .

to its starting point  $p(t)$ , given by Eq. (7). Here we choose  $N = 1000$ ,  $S = 1000$  and the minimum and the maximum allowed degrees are  $K_{\min} = 2$  and  $K_{\max} = 999$ , respectively. The asymptotic behavior of the classical average probability at very long times is well recovered for all networks. The long-time behavior depends only on the number of nodes,  $N$ , thus it is independent of their topology. Similar findings were also encountered in Ref. [94], in which the long-time behavior of random walks is influenced mainly by the minimum degree of their vertices. In our model for a star the equipartition value  $1/N$  is reached at  $t_{eq} \approx 11$  and for a linear chain we reach it at  $t_{eq} \approx 5 \times 10^5$ , not shown in the figure due to its extremely high value. For GSFNs  $t_{eq}$  has values between the two above-mentioned limits, with lower values for networks with more starlike segments, i.e., lower  $\gamma$ 's. In the intermediate-time domain the average probability follows a power-law decay  $p(t) \propto t^{-\alpha}$  with the exponent  $\alpha$  varying from 0.38, obtained for GSFNs with  $\gamma = 1.0$ , until 0.77, which was encountered for GSFNs with  $\gamma = 4.0$ . For a single linear chain one also gets a power-law decay with exponent  $\alpha = 0.5$ , while for a star with  $N - 1$  arms there is no intermediate-time behavior, only a step decay. For very short times ( $t \leq 10^0$ ) the situation changes: we encounter an exponential decay  $p(t) \propto e^{-\beta t}$  for

the star and GSFNs with  $\gamma \leq 2.0$  and an inverse function  $p(t) \propto \frac{1}{1+\epsilon t}$  as the best fit for the linear chain and GSFNs with  $\gamma > 2.0$ . For a pure star and GSFNs with  $\gamma = 1$  we found  $\beta = 0.98$  and for GSFNs with  $\gamma = 2.0$  we have  $\beta = 0.92$ , while for the linear chain we found  $\epsilon = 2.27$  and for other GSFNs we have  $(\gamma, \epsilon) = (2.5, 1.71)$ ,  $(3.0, 1.77)$ , and  $(4.0, 1.96)$ .

In Fig. 4(b) we keep the parameter  $\gamma$  constant at 2.5 and we vary the size of the stars by increasing the value of  $K_{\min}$ . The behavior of the classical probability, Eq. (7), is strongly influenced by the eigenvalue spectrum, shown in Fig. 3(b). The convergence towards the equipartition value is governed by the lowest nonvanishing eigenvalue  $\lambda_2$ , known as spectral gap [77]: the larger  $\lambda_2$ , the faster the decay. For our choice of parameters the spectral gap does not differ too much, for instance  $\lambda_2 = 0.0010$  for  $K_{\min} = 2$  to  $\lambda_2 = 0.0016$  for  $K_{\min} = 10$ , which explains why the results are similar in the intermediate-time region. For higher values of  $K_{\min}$  the average probability  $p(t)$  of a walker returning to the initial node gets lower. By increasing the size of the minimum allowed degree  $K_{\min}$  we slowly destroy the power-law behavior in the region of low intermediate times and there emerges a small peak, which resembles the steep decay observed in Fig. 4(a) for a single star. However, this behavior extends

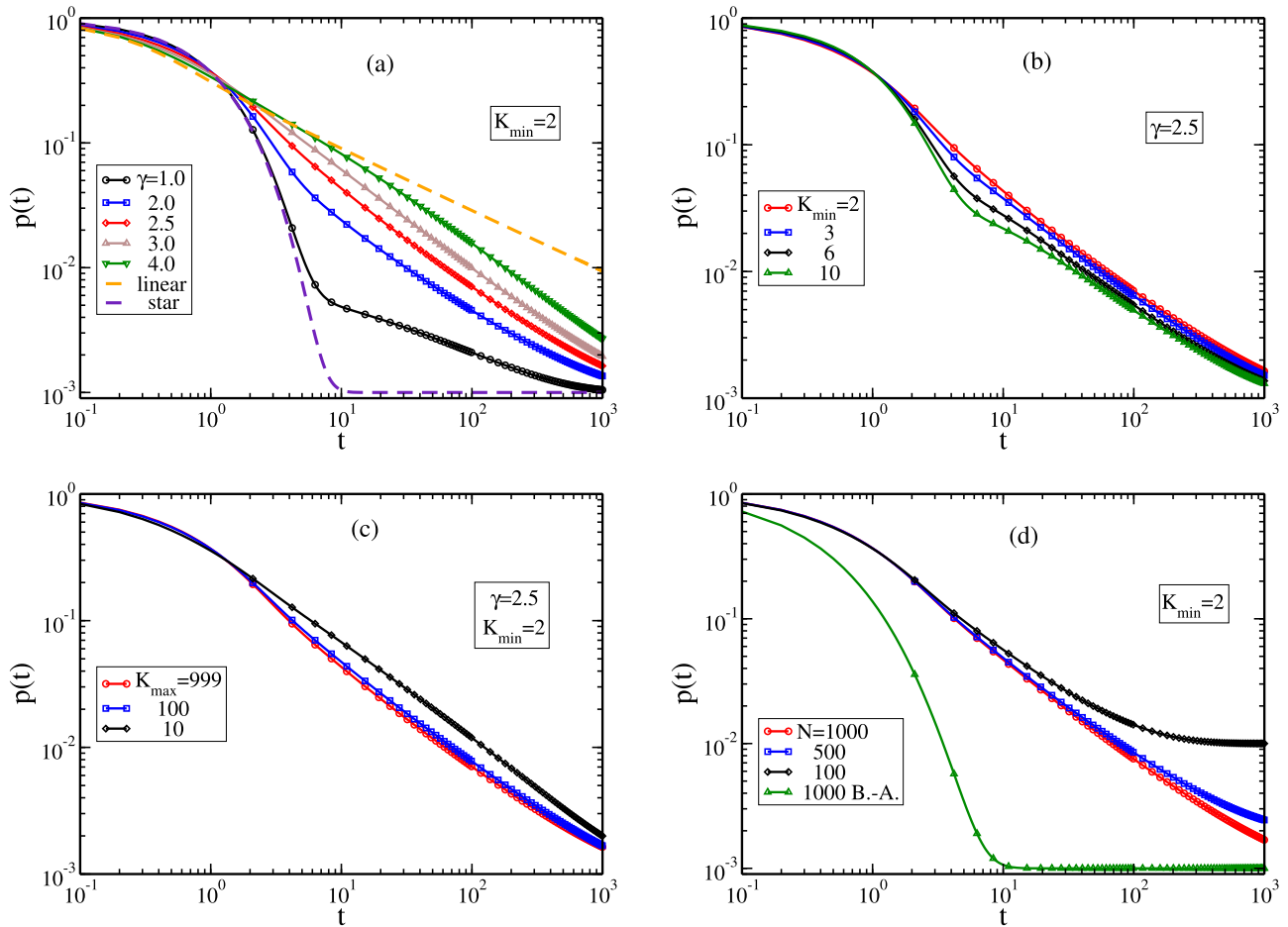


FIG. 4. Classical probability  $p(t)$  of returning to the starting node as a function of time  $t$  for GSFNs with  $N = 1000$ ,  $S = 1000$ , and the parameters  $(\gamma, K_{\min}, K_{\max})$ : (a) (variable, 2, 999), (b) (2.5, variable, 999), and (c) (2.5, 2, variable). In (d)  $N$  and  $S$  are varied and  $\gamma = 2.6$ ,  $K_{\min} = 2$ , and  $K_{\max} = N - 1$ .

for only one order of magnitude and it can be related to the degeneracy of eigenvalue 1 and the width of the gap between this eigenvalue and the next one. This gap enlarges when  $K_{\min}$  increases, as shown in Fig. 3(b) and highlighted in Fig. 5 of Ref. [82]. Similar findings were encountered for all values of the parameters  $\gamma$  and  $K_{\max}$ , while only  $K_{\min}$  is varied.

In Fig. 4(c) we monitor the influence of the maximum allowed degree  $K_{\max}$  on the probability  $p(t)$ . Here we consider  $\gamma = 2.5$  and  $K_{\min} = 2$ , thus in the limiting case,  $K_{\min} = K_{\max}$ , we obtain a pure linear chain. Here, like in all previous panels, we are mainly interested in the intermediate-time region, which is the only region with different behavior. Remarkably, we observed that by decreasing  $K_{\max}$  the probability  $p(t)$  gets higher and the power-law exponent in the intermediate-time region keeps the same value, 0.76, but this behavior gets broader. This is due to an increase in the length of the linear segments, which also explains the similarity with the behavior of a single linear chain, shown in Fig. 4(a). From the perspective of the eigenvalue spectrum, see Fig. 3(c), this change can be directly related to the highest degenerate eigenvalue,  $\lambda = 1$ .

In Fig. 4(d) we vary the size of our networks,  $N$ , keeping constant the other parameters:  $(\gamma, K_{\min}, K_{\max}) = (2.6, 2, N - 1)$ . Here, we also realize a comparison between scale-free networks constructed from our treelike GSFN algorithm and

from the model of Barabási-Albert [80], which provides networks with loops. One can easily notice that networks with loops reach the equipartition constant value  $1/N$  faster and the time difference is extended over more than three orders of magnitude. Due to a higher number of links between nodes, with some of them having a very high degree, the probability of returning is lower in the Barabási-Albert model, i.e., the spreading on networks is more effective. This behavior is similar to a single star or to GSFNs with high  $K_{\min}$ .

## D. Quantum transport

### 1. Spacetime structures

In Fig. 5 we display the contour plots of the quantum return probability  $\pi$  for three particular realizations of the GSFN algorithm. These networks with  $N = 100$  nodes are depicted in Figs. 1(a), 1(d), and 1(f), in which we show also the nodes' number to facilitate a better understanding of the results. In the left column, Figs. 5(a), 5(d), and 5(g), we show the results of a network with  $(\gamma, K_{\min}, K_{\max}) = (1, 2, 99)$ ; in the middle column, Figs. 5(b), 5(e), and 5(h), we have the network with the parameter set (2.5, 2, 99); and in the right column, Figs. 5(c), 5(f), and 5(i), the network is for (2.5, 6, 99). For the sake of comparison we show the same quantum probabilities

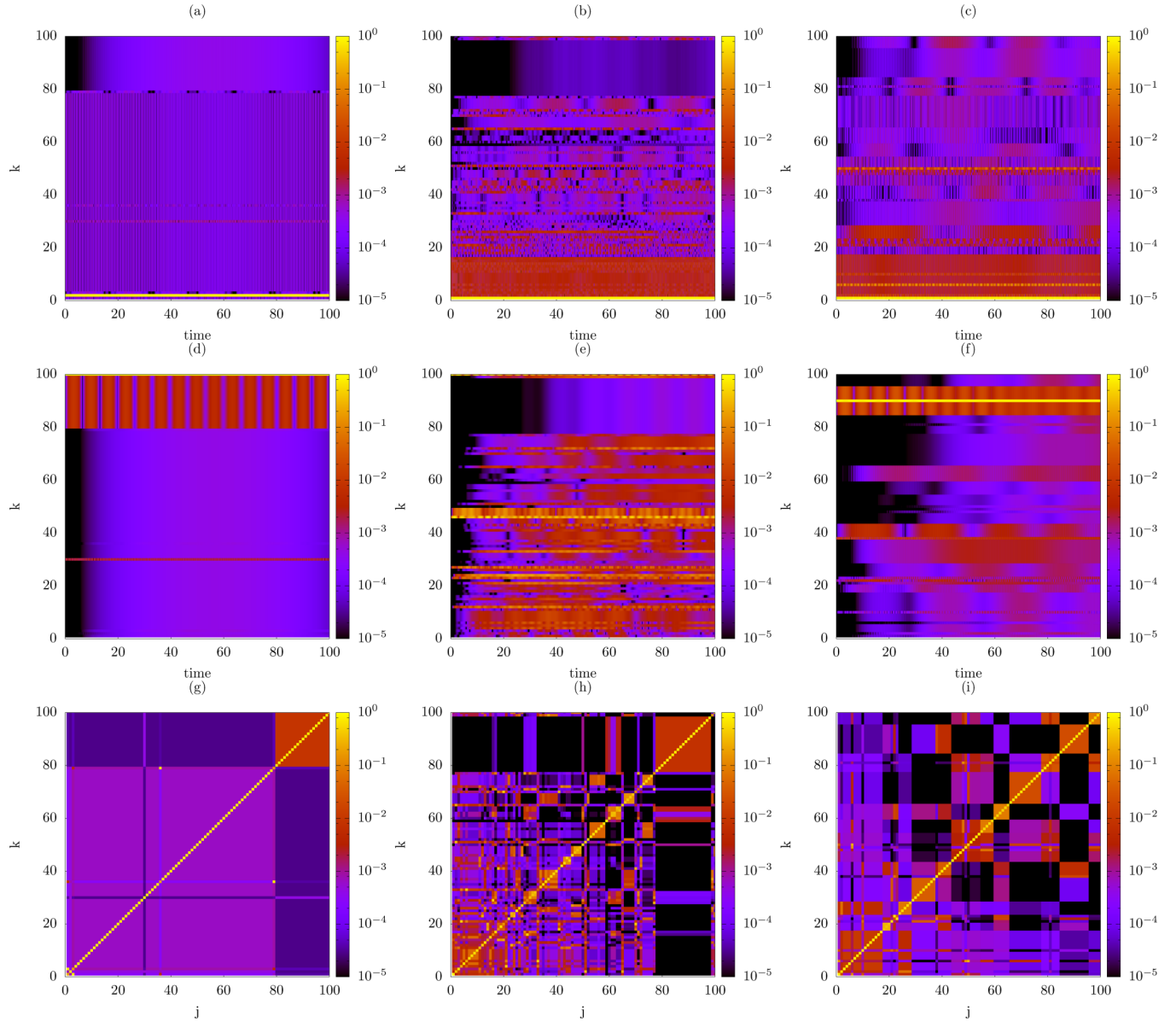


FIG. 5. Spacetime structures for three GSFNs displayed in Fig. 1, more exactly Fig. 1(a) (left column), Fig. 1(d) (middle column), and Fig. 1(f) (right column). The rows correspond to  $\pi_{k,center}(t)$  (top row),  $\pi_{k,periphery}(t)$  (middle row), and  $\pi_{j,k}(t = 10)$  (bottom row).

for the three networks. Immediately apparent is the symmetry of the figures,  $\pi_{j,k} = \pi_{k,j}$ , which is a direct consequence of the model; see Eq. (4). In the first row, Figs. 5(a)–5(c), we consider the time evolution of the probabilities from the center of each network, depicted by red squares in Fig. 1, to all nodes,  $\pi_{k,center}(t)$ .

In Fig. 5(a) the center is node 2, which is the node with the highest transition probability for all time values. Node 2 is the core of a star with 76 neighbors and, as is known from the literature [83,84,95], in the quantum case the stars show high localization effects, which explains our findings. The neighbors of node 2, namely the nodes 1 and 4–78, show higher probabilities for various time values. The second highest probabilities are found for  $\pi_{30,2}$ , which correspond to the walker being at the core of the second big star of our network. The probabilities of reaching the second-order

neighbors, depicted by black in the figure, are smaller for almost all time values. It is worth stressing that in the case of single stars when the quantum walk starts at the core it can be mapped into a walk involving only two nodes [83,96]. However, when the walks starts at a peripheral node, we do not have such a simple mapping.

In Fig. 5(b) the center is node 1 and it corresponds to a network with smaller stars, but longer linear segments: its diameter equals 11. The highest probability continues to be  $\pi_{1,1}$ , due to the fact that node 1 is the core of a star with 16 arms. However, for almost all time values we have high probability of the walker going to these sixteen next-nearest neighbors. We found relatively high probabilities of reaching more distant nodes, due to an increase of the linear segments. Similarly to the previous network, the lowest probabilities correspond to peripheral nodes, i.e., displayed by indigo in

Fig. 1(d). Overall we can state that the spreading of the quantum walker is much more efficient for this network.

In Fig. 5(c) the center is node 1 and the network is composed of small coupled stars. This network has its diameter equal to 8, lower than the previous network, but it contains more nodes with degree higher than 5, more exactly 12 nodes. This mixture of linear segments and high degree nodes has strong influence on quantum transport. We notice a not trivial combination between localization effects and good spreading. The localization effects, due to the starlike segments, are better seen usually on the next-nearest neighbors of the center and at the cores of the stars. At the same time the probability of reaching the peripheral nodes is not as low as in the previous cases, due to the linear segments.

In the second row of Fig. 5 we focus on the transition probabilities from a peripheral node, which in our case is chosen to be one of the most distant nodes from the center. This node is chosen to be 100 for networks shown in Figs. 1(a) and 1(d) and node 90 for the network displayed in Fig. 1(f). In Fig. 5(d) we have as the highest probability  $\pi_{100,100}$ , followed by the probability of the transition from the peripheral node 100 to its nearest neighbor, node 30. For almost all time values  $\pi_{30,100}$  is the second highest probability. This probability is followed by the probabilities of visiting the second-nearest neighbors, namely nodes 29 and 80–99. These results are perfectly explained by the topology of the network: practically, two stars are coupled through link (2,30). Thus, the localization effects are more pronounced if the walker starts from the periphery than from the core of one of the stars.

In Fig. 5(e) we focus on network Fig. 1(d) and we choose a peripheral node that belongs to a linear segment, namely node 100. Although it is not exactly the most distant node from the center we choose this node also for being opposite to the largest star, which has node 59 as its core. Due to a significant increase of the longest linear path we encountered higher transition probabilities not only for the next-nearest neighbors, but also for distant nodes. For instance for node 72, which is a neighbor of ninth order, we get  $\pi \approx 0.1$  for various time values. This can be explained by the fact that the shortest path linking node 100 to node 72 passes only through a single big star. Similar results were found for nodes with the shortest path to node 100 mainly composed of linear segments, for instance the nodes 24, 45, to name only a few. We still get low probabilities of transitions from node 100 to one of the nodes of the opposite star along the network, namely nodes 78–98. One concludes that for this network the quantum transport is more effective, starting from any node of the network.

In Fig. 5(f) we display the time evolution of the transition probabilities from the peripheral node 90, which belongs to one of the stars. Our chosen network is composed of twelve coupled stars, the longest linear segment being the backbone that links almost all of them. This fact provides a mixture of strong localization effects, due to the starlike parts, and good spreading, a consequence of the linear segments. We found the highest probabilities for transitions from node 90 to nodes belonging to the same star. However, for time values higher than 80 we encounter a more homogeneous situation, where almost all the probabilities are higher than  $10^{-4}$ . A possible visualization for this behavior is the following: the walker reaches a star, it stays localized to this new star, and after

awhile it goes to the next star. This process is repeated until the quantum walker visits all the stars.

In the last row of Fig. 5 we fixed the time value to  $t = 10$  and we compute all the transition probabilities  $\pi_{j,k}$  between all possible pairs. However, it is important to stress that qualitatively we have a similar behavior for any value of time. For our three considered networks we obtained very high probabilities of returning to the initial node. For the network displayed in Fig. 1(a) we observed strong localization effects. The probabilities are higher than  $10^{-4}$  only for transitions between nodes belonging to the same star. For network Fig. 1(d) we observed a better mixture between localization effects and good spreading over the whole network. The highest probabilities are between nodes belonging to the same star and the lowest probabilities are between nodes from two different and distant stars, for instance the stars with cores 1 and 59. Due to a higher density of linear segments the nodes from the star with core 1 show a better spreading. From a pure visualization perspective these contour plots can ease our way in determining the number of stars from a network. The same aspect can be observed in Fig. 5(i): the number of orange-red colored blocks along the main diagonal gives us a good idea of how many stars, i.e., nodes with high degree, we are dealing with. As in the previous two panels related to this network, Figs. 1(c) and 1(f), we noticed a better mixture between two extreme behaviors: a linear chain and a star.

## 2. Average return probabilities

Now we turn our attention to quantum mechanical transport over GSFNs. In Fig. 6 we focus on the quantum average probability  $\bar{\pi}(t)$ , given by Eqs. (4) and (6). In Fig. 6(a) we compare the quantum average probability with the classical return probability  $p(t)$ , Eq. (7), and the lower bound  $\bar{\alpha}(t)$ , Eq. (8), for GSFNs with  $\gamma = 1.0$  and 4.0. The minimum and the maximum allowed degrees are fixed to  $K_{\min} = 2$  and  $K_{\max} = 999$ , respectively. For GSFNs with  $\gamma = 1.0$ , which correspond to networks with predominant starlike topology, in the quantum case the walks experience strong localization effects, thus the average probability of returning to the starting node is high. This fact is evident also from our considered quantum probabilities, for which the values fluctuate around 0.98 (for  $\bar{\pi}$ ) and 0.96 (for  $\bar{\alpha}$ ). The classical probability is almost three orders of magnitude lower than its quantum counterpart and it shows a different time-decay behavior. It is important to mention that a quantum walker on large stars has a higher probability of returning to the starting node than the classical walker. For all structures we obtain that in the long-time limit the classical return probability equals  $1/N$ . In the quantum case the probability oscillates around a certain value, which can be higher than  $1/N$ . One should not conclude that CTRW is faster than CTQW, but this fact only means that in the long-time limit the probability is equally distributed among all nodes [95]. This result is a consequence of having one highly degenerate eigenvalue in both cases. For networks with more linear segments,  $\gamma = 4.0$ , the quantum transport increases significantly, but the localization effects are still present. For these GSFNs both quantum probabilities show larger fluctuations, but they reach the long-time average value faster, comparing with the classical probability. By further

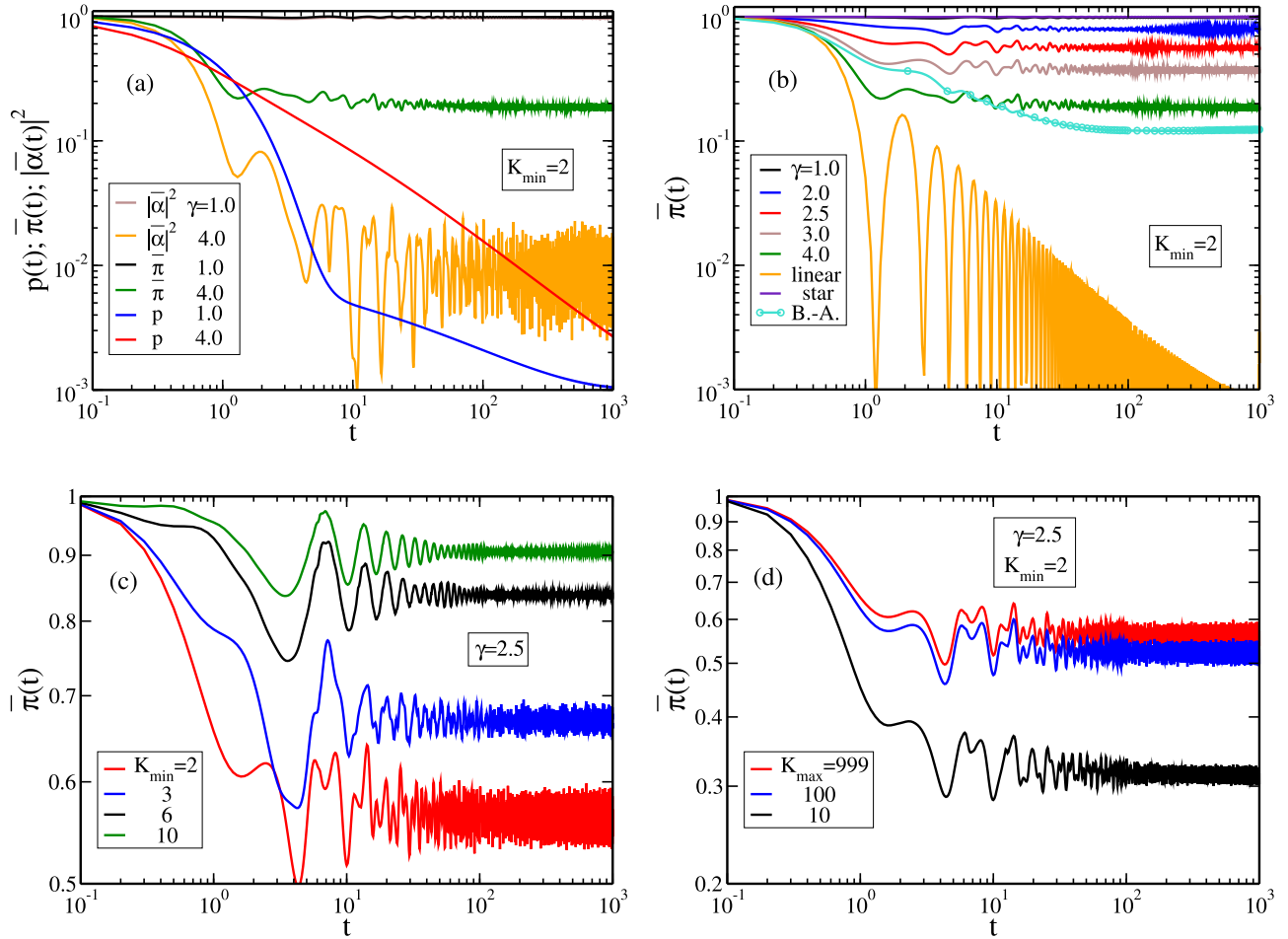


FIG. 6. Quantum average return probability  $\bar{\pi}(t)$  as a function of time  $t$ , Eq. (8), for  $S = 1000$  GSFNs with  $N = 1000$  nodes. (a) Comparison between classical and quantum probabilities for networks with  $K_{\min} = 2$ ,  $K_{\max} = 999$ , and  $\gamma = 1$  and  $4$ . (b) Quantum probability for networks with  $\gamma$  variable and  $(K_{\min}, K_{\max}) = (2, 999)$ . (c)  $\bar{\pi}(t)$  for GSFNs with  $\gamma = 2.5$ ,  $K_{\max} = 999$ , and  $K_{\min}$  variable. (d)  $\bar{\pi}(t)$  for GSFNs with  $\gamma = 2.5$ ,  $K_{\min} = 999$ , and  $K_{\max}$  variable.

increasing the value of  $\gamma$  we increase the linear segments and we obtain stronger fluctuations for the quantum average probabilities. In the limiting case, namely a single linear chain, one encounters an important increase in efficiency for CTQW, because the quantum probability of returning,  $\bar{\pi}(t)$ , decays faster than for CTRW [83]. In the region of intermediate times the CTRW follows a  $t^{-1/2}$  decay, while the CTQW scales with  $t^{-1}$ .

In Fig. 6(b) we show how the networks' topology influences the quantum average return probability  $\bar{\pi}(t)$ . Here, we display also the results for our extreme cases: a single linear chain and a star with  $N - 1$  arms, and additionally the original Barabasi-Albert scale-free network [80]. All scale-free networks show decays between the two extreme cases, more precisely strong localization for a star and good spreading for a linear chain. All GSFNs reach the long-time average value faster and the fluctuations around this value become lower by increasing  $\gamma$ . However for very high  $\gamma$ , the GSFNs approach a single linear chain situation, for which the big fluctuations get higher. We notice that the increase in the quantum efficiency is not that considerable, when  $\gamma$  grows. For instance, in the long-time limit the quantum probability fluctuates around the value 0.98 for  $\gamma = 1.0$  and 0.18 for  $\gamma = 4.0$ . This is a conse-

quence of the fact that even for high  $\gamma$  the number of nodes with high degree is enough to prevail the localization effects. An interesting situation occurs when we compare to the B.-A. model's networks, which contain loops and have a higher total number of links. Remarkably, for B.-A. networks the quantum average probability  $\bar{\pi}$  is lower than all considered GSFNs, although its power-law exponent equals 2.64. The treelike GSFNs with a similar exponent,  $\gamma = 2.5$ , display higher probabilities meaning that the localization effects are stronger. For B.-A. networks also the fluctuations around the equilibrium value 0.12, which is almost two orders of magnitude lower than the classical limit  $\frac{1}{N}$ , are practically nonexistent. However, the B.-A. networks are delayed in reaching their long-time average value if we compare to GSFNs. All these properties are due to the presence of loops, which increase the number of linear segments and the total number of links.

In Fig. 6(c) we monitor the influence of  $K_{\min}$  on the quantum average probability for GSFNs with fixed  $\gamma = 2.5$  and  $K_{\max} = 999$ . Immediately apparent is an increase of  $\bar{\pi}$  when the minimum allowed degree gets higher. GSFNs composed of bigger stars show a more prominent localization effect. Regarding the long-time average value, we observe that it is reached almost at the same time. However, this probability

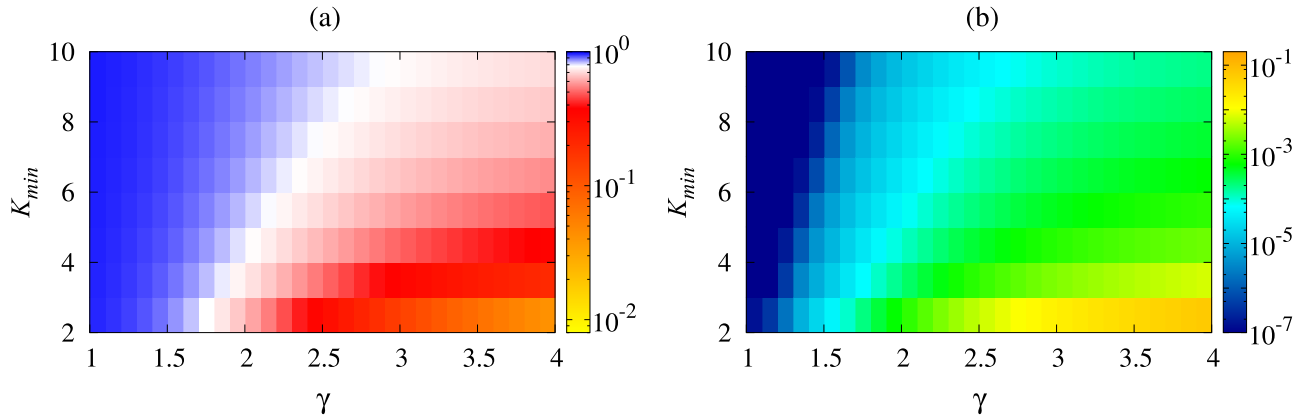


FIG. 7. Long-time average probability  $\chi$  (a) and the relative difference  $(\chi - \chi^*)/\chi$  (b) for GSFNs with  $N = 1000$ ,  $S = 1000$ , and  $K_{\max} = 999$  as function of  $\gamma$  and  $K_{\min}$ .

gets almost double when  $K_{\min}$  grows from 2 to 10, more exactly  $\bar{\pi} \approx 0.55$  to  $\bar{\pi} \approx 0.90$ . We also notice that the strength of the fluctuations around the long-time average are drastically diminished when the minimum size of the stars gets higher. This fact can be also inferred if one compares  $\bar{\pi}$  of a single chain and a star with  $N - 2$  arms, both curves being shown in Fig. 6(b). The behavior of a linear chain is governed by large fluctuations while for a star they are extremely small.

In Fig. 6(d) we vary the maximum allowed degree  $K_{\max}$  and we keep constant the other parameters:  $\gamma = 2.5$  and  $K_{\min} = 2$ . GSFNs with lower  $K_{\max}$  will increase the spreading over networks due to an increase in the size of linear segments. However, differently than other parameters,  $K_{\max}$  shows a weaker influence on the long-time average value and on the strength of the fluctuations around this value. This is similar to the classical probability, and the weak influence on  $K_{\max}$  does not reside in the sizes of the stars, but in the matter of having a network composed of stars.

In Fig. 7 we focus on the quantum transport efficiency and we measure the long-time average  $\chi$  (left panel) and the relative difference  $(\chi - \chi^*)/\chi$  (right panel), where the approximation  $\chi^*$  is given by Eq. (10). Here, we fix  $K_{\max}$  to  $N - 1 = 999$  and we consider  $S = 1000$  GSFN realizations for each value of the parameter set  $(\gamma, K_{\min})$ . We choose to display the results in a two-dimensional map, in which the efficiency strength is represented by colors. The long-time average  $\chi$  has values between 0 and 1. The quantum transport is considered to be efficient if  $\chi$  is low, with the maximum efficiency being reached when  $\chi = 0$ . The transport is less efficient if  $\chi$  is high, with the maximum inefficiency being encountered when  $\chi = 1$ . From Eq. (10) we can state that the quantum transport gets better, i.e., lower values of  $\chi$ , when  $\gamma$  increases. This property is valid for all values of  $K_{\min}$  with other parameters being fixed. For GSFNs with  $K_{\min} = 2$  we improve the efficiency of the transport by almost two orders of magnitude by increasing  $\gamma$  from 1 to 4, namely  $\chi(\gamma = 1, K_{\min} = 2) = 0.96$  and  $\chi(4, 2) = 0.012$ . In the same manner one observes a decrease of quantum efficiency when  $K_{\min}$  increases while  $\gamma$  is kept constant. All these findings are directly related to the quantities of stars and linear segments existing in GSFNs. Remarkably, we obtain the same quantum efficiency for various values of the parameter set  $(\gamma, K_{\min})$ ,

although the topology of the networks is vastly different. For a better understanding of this statement one could follow the white color in Fig. 7(a), which correspond to  $\chi \approx 0.7$ . For example, the quantum efficiency is almost the same for the parameter sets (1.8,2), (2.0,3), (2.4,5), and (2.6,6), to name only a few. Practically, for every  $\gamma$  value one finds a proper value of  $K_{\min}$  that will give the same  $\chi$ . Similar results are obtained for all values of  $\chi$ ; only the values of the considered parameters change. Regarding the approximate  $\chi^*$  values, we encounter a behavior similar to the exact values  $\chi$ , not shown here. This can be seen from Fig. 7(b), where for a better visualization we show the relative difference between the exact and the approximate long-time average probabilities:  $(\chi - \chi^*)/\chi$ . The difference between them is at maximum 20% and around 1% on average. Thus, for these networks the approximation holds [89,90], which is mainly due to a predominantly discrete nature of the eigenvalue spectrum of our GSFNs.

## V. CONCLUSIONS

In this article we have studied continuous-time quantum walks on generalized scale-free networks. These networks were constructed in a treelike manner by making use of a growth mechanism [82]. The degree distribution followed a power law with its exponent  $\gamma$  being chosen at the beginning of the procedure. Additionally, we have considered two modularity parameters, which enhanced the quantum transport by a proper choice of their values: the minimum allowed degree,  $K_{\min}$ , and the maximum allowed degree,  $K_{\max}$ . We have constructed finite-size treelike networks, meaning that all networks contain nodes with degree 1, i.e., the peripheral nodes. In this article we have monitored how classical and quantum transport are influenced by the above-mentioned parameters. We have chosen as quantities of interest the average return probability and the long-time average transition probability  $\chi$ . In the continuous-time model these probabilities are reduced to the complete determination of the eigenvalues and the eigenvectors of the connectivity matrix. The eigenvalue spectrum shows a stronger dependence on  $\gamma$  than on the other two parameters. At the same time, a change of parameter  $K_{\min}$  is more effective in switching the topology of the networks

towards a more starlike shape than changing  $K_{\max}$ . Another important feature, which is more evident for lower  $\gamma$ s, is a decrease in the degeneracy of the eigenvalue  $\lambda = 1$  when  $K_{\max}$  gets lower. This fact is related to an increase of the size of linear segments.

Both classical and quantum transport on GSFNs have shown a behavior between two extreme cases: a pure linear chain and a single star with  $N - 1$  arms. In the classical situation GSFNs with a predominantly starlike topology revealed a better transport, while for linear chains the spreading on the network is slow. In the intermediate-time domain GSFNs showed a power-law decay with exponents between 0.38 (for  $\gamma = 1.0$ ) and 0.77 (for  $\gamma = 4.0$ ). By further increasing the value of  $\gamma$  we encounter in the intermediate region a more linearlike behavior, having in the limit of  $\gamma \rightarrow \infty$  a pure linear chain behavior, namely a power law with exponent equal to 0.5. All CTRWs on networks will eventually decay in the long-time limit to the equipartition value  $1/N$ . The transport is considered to be more efficient if the above mentioned value is reached faster. Thus, if we are looking for scale-free networks with a good (uniform) and fast spreading we should aim towards GSFNs composed of larger stars. Here, we have shown that there are two mechanisms to do this: decrease the value of  $\gamma$  or increase the minimum allowed degree  $K_{\min}$ .

In the quantum case the situation is different: the efficiency of the transport, measured through the long-time average probability, is better for linear chains than stars. For stars the localization effects are strong: the walkers usually stay

in the neighborhood of the starting node. However, the equilibrium situation is reached quicker by networks with more starlike topology. For this type of network we have noticed a significant decrease of the fluctuations' strength around the average efficiency value. Remarkably, we have found that the same quantum efficiency is encountered for various pairs of the parameter set  $(\gamma, K_{\min})$ , i.e., different topologies. More precisely, for every value of  $K_{\min}$  one finds a value of  $\gamma$  which gives the same  $\chi$ . We have shown that the strong quantum localization effects can be overcome by increasing the value of  $\gamma$  while the other parameters are kept constant. Another mechanism to increase the quantum efficiency is by decreasing the maximum allowed degree  $K_{\max}$ , but increasing the minimum allowed degree  $K_{\min}$  yields the opposite effect: a decrease in the efficiency. Thus, we can state that the quantum efficiency is optimized by increasing the value of  $\gamma$ , by decreasing  $K_{\min}$ , or by increasing  $K_{\max}$ , having the pure linear chain as their upper limit. We have noticed that the speed in reaching the quantum average long-time return probability does not depend too much on our construction parameters  $\gamma$ ,  $K_{\min}$ , and  $K_{\max}$ , but it is mainly related to the total number of links.

#### ACKNOWLEDGMENTS

C.M.M. acknowledges the financial support of CAPES (Brazil) and FAPEAM (Brazil). M.G. is grateful to CNPq (Brazil) for financial support.

- 
- [1] G. H. Weiss, *Aspects and Applications of the Random Walk* (North-Holland, Amsterdam, 1994).
  - [2] N. Van Kampen, *Stochastic Processes in Physics and Chemistry* (North-Holland, Amsterdam, 2011).
  - [3] J. Rudnick and G. Gaspari, *Elements of the Random Walk: An Introduction for Advanced Students and Researchers* (Cambridge University Press, Cambridge, 2004).
  - [4] R. Klages, G. Radons, and I. M. Sokolov, *Anomalous Transport: Foundations and Applications* (Wiley-VCH, Weinheim, 2008).
  - [5] J. Klafter and I. M. Sokolov, *First Steps in Random Walks: From Tools to Applications* (Oxford University Press, Oxford, 2011).
  - [6] A. Baronchelli, M. Catanzaro, and R. Pastor-Satorras, Random walks on complex trees, *Phys. Rev. E* **78**, 011114 (2008).
  - [7] J. D. Noh and H. Rieger, Random Walks on Complex Networks, *Phys. Rev. Lett.* **92**, 118701 (2004).
  - [8] M. Doi and S. R. Edwards, *The Theory of Polymer Dynamics* (Clarendon, Oxford, 1986).
  - [9] T. Aquino and M. Dentz, Chemical Continuous Time Random Walks, *Phys. Rev. Lett.* **119**, 230601 (2017).
  - [10] O. Bénichou and R. Voituriez, From first-passage times of random walks in confinement to geometry-controlled kinetics, *Phys. Rep.* **539**, 225 (2014).
  - [11] E. Eisenberg, S. Havlin, and G. H. Weiss, Fluctuations of the Probability Density of Diffusing Particles for Different Realizations of a Random Medium, *Phys. Rev. Lett.* **72**, 2827 (1994).
  - [12] J.-P. Bouchaud and A. Georges, Anomalous diffusion in disordered media: Statistical mechanisms, models and physical applications, *Phys. Rep.* **195**, 127 (1990).
  - [13] N. Masuda, M. A. Porter, and R. Lambiotte, Random walks and diffusion on networks, *Phys. Rep.* **716-717**, 1 (2017).
  - [14] R. Pastor-Satorras, C. Castellano, P. van Mieghem, and A. Vespignani, Epidemic processes in complex networks, *Rev. Mod. Phys.* **87**, 925 (2015).
  - [15] F. Iannelli, A. Koher, D. Brockmann, P. Hövel, and I. M. Sokolov, Effective distances for epidemics spreading on complex networks, *Phys. Rev. E* **95**, 012313 (2017).
  - [16] G. Ritschel, J. Roden, W. T. Strunz, A. Aspuru-Guzik, and A. Eisfeld, Absence of quantum oscillations and dependence on site energies in electronic excitation transfer in the Fenna-Matthews-Olson trimer, *J. Phys. Chem. Lett.* **2**, 2912 (2011).
  - [17] G. Ritschel, J. Roden, W. T. Strunz, and A. Eisfeld, An efficient method to calculate excitation energy transfer in light-harvesting systems: Application to the Fenna-Matthews-Olson complex, *New J. Phys.* **13**, 113034 (2011).
  - [18] V. M. Kenkre and P. Reineker, *Exciton Dynamics in Molecular Crystals and Aggregates* (Springer, Berlin, 1982).
  - [19] W. M. Zhang, T. Meier, V. Chernyak, and S. Mukamel, Exciton-migration and three-pulse femtosecond optical spectroscopies of photosynthetic antenna complexes, *J. Chem Phys.* **108**, 7763 (1998).
  - [20] K. Hyeon-Deuk, Y. Tanimura, and M. Cho, Ultrafast exciton-exciton coherent transfer in molecular aggregates and its application to light-harvesting systems, *J. Chem Phys.* **127**, 075101 (2007).
  - [21] P. Rivera, K. L. Seyler, H. Yu, J. R. Schaibley, J. Yan, D. G. Mandrus, W. Yao, and X. Xu, Valley-polarized exciton

- dynamics in a 2D semiconductor heterostructure, *Science* **351**, 688 (2016).
- [22] C. K. Lee, L. Shi, and A. P. Willard, A model of charge-transfer excitons: Diffusion, spin dynamics, and magnetic field effects, *J. Phys. Chem. Lett.* **7**, 2246 (2016).
- [23] B.-X. Wang, M.-J. Tao, Q. Ai, T. Xin, N. Lambert, D. Ruan, Y.-C. Cheng, F. Nori, F.-G. Deng, and G.-L. Long, Efficient quantum simulation of photosynthetic light harvesting, *npj Quantum Inf.* **4**, 52 (2018).
- [24] F. Fassioli, R. Dinshaw, P. C. Arpin, and G. D. Scholes, Photosynthetic light harvesting: Excitons and coherence, *J. R. Soc. Interface* **11**, 20130901 (2014).
- [25] T. Brixner, R. Hildner, J. Köhler, C. Lambert, and F. Würthner, Excitonic natural antennas to synthetic chromophore systems—From natural antennas to synthetic chromophore systems, *Adv. Energy Mater.* **7**, 1700236 (2017).
- [26] A. Drinko, F. M. Andrade, and D. Bazeia, Narrow peaks of full transmission in simple quantum graphs, *Phys. Rev. A* **100**, 062117 (2019).
- [27] G. Berkolaiko and P. Kuchment, *Introduction to Quantum Graphs* (American Mathematical Society, Providence, 2012).
- [28] A. A. Zhukov, S. V. Remizov, W. V. Pogosov, and Yu. E. Lozovik, Algorithmic simulation of far-from-equilibrium dynamics using quantum computer, *Quantum Inf. Process.* **17**, 223 (2018).
- [29] J. M. Harrison and E. Swindle, Spectral properties of quantum circulant graphs, *J. Phys. A: Math. Theor.* **52**, 285101 (2019).
- [30] S. Severini and G. Tanner, Regular quantum graphs, *J. Phys. A: Math. Gen.* **37**, 6675 (2004).
- [31] M. Mosca, *Encyclopedia of Complexity and Systems Science* (Springer, New York, 2009).
- [32] A. M. Childs, Universal Computation by Quantum Walk, *Phys. Rev. Lett.* **102**, 180501 (2009).
- [33] C. D. Bruzewicz, J. Chiaverini, R. McConnell, and J. M. Sage, Trapped-ion quantum computing: Progress and challenges, *Appl. Phys. Rev.* **6**, 021314 (2019).
- [34] P. Schindler *et al.*, A quantum information processor with trapped ions, *New J. Phys.* **15**, 123012 (2013).
- [35] M. Nielsen and I. Chuang, *Quantum Computation and Quantum Information* (Cambridge University Press, Cambridge, 2000).
- [36] I. M. Georgescu, S. Ashhab, and F. Nori, Quantum simulation, *Rev. Mod. Phys.* **86**, 153 (2014).
- [37] R. Portugal, *Quantum Walks and Search Algorithms* (Springer, New York, 2013).
- [38] A. M. Childs and J. Goldstone, Spatial search by quantum walk, *Phys. Rev. A* **70**, 022314 (2004).
- [39] M. Cattaneo, M. A. C. Rossi, M. G. A. Paris, and S. Maniscalco, Quantum spatial search on graphs subject to dynamical noise, *Phys. Rev. A* **98**, 052347 (2018).
- [40] L. K. Grover, Quantum Mechanics Helps in Searching for a Needle in a Haystack, *Phys. Rev. Lett.* **79**, 325 (1997).
- [41] P. W. Shor, Algorithms for quantum computation: Discrete logarithms and factoring, in *35th IEEE Symposium on Foundations of Computer Science, Los Alamos, 1994* (IEEE, Piscataway, NJ, 1994), p. 124.
- [42] B. Hein and G. Tanner, Quantum search algorithms on a regular lattice, *Phys. Rev. A* **82**, 012326 (2010).
- [43] I. Foulger, S. Gnutzmann, and G. Tanner, Quantum Search on Graphene Lattices, *Phys. Rev. Lett.* **112**, 070504 (2014).
- [44] C. Gross and I. Bloch, Quantum simulations with ultracold atoms in optical lattices, *Science* **357**, 995 (2017).
- [45] M. Lewenstein, A. Sanpera, and V. Ahufinger, *Ultracold Atoms in Optical Lattices* (Oxford University Press, Oxford, 2012).
- [46] B. C. Sanders, S. D. Bartlett, B. Tregenna, and P. L. Knight, Quantum quincunx in cavity quantum electrodynamics, *Phys. Rev. A* **67**, 042305 (2003).
- [47] C. J. Axline, L. D. Burkhardt, W. Pfaff *et al.*, On-demand quantum state transfer and entanglement between remote microwave cavity memories, *Nat. Phys.* **14**, 705 (2018).
- [48] R. Côté, A. Russel, E. E. Eyler, and P. L. Gould, Quantum random walk with Rydberg atoms in an optical lattice, *New J. Phys.* **8**, 156 (2006).
- [49] O. Mülken, A. Blumen, T. Amthor, C. Giese, M. Reetz-Lamour, and M. Weidemüller, Survival Probabilities in Coherent Exciton Transfer with Trapping, *Phys. Rev. Lett.* **99**, 090601 (2007).
- [50] C. S. Adams, J. D. Pritchard, and J. P. Shaffer, Rydberg atom quantum technologies, *J. Phys. B: At. Mol. Opt. Phys.* **53**, 012002 (2020).
- [51] W. Dür, R. Raussendorf, V. M. Kendon, and H.-J. Briegel, Quantum walks in optical lattices, *Phys. Rev. A* **66**, 052319 (2002).
- [52] M. Karski, L. Forster, J. M. Choi, A. Steffen, W. Alt, D. Meschede, and A. Widera, Quantum walk in position space with single optically trapped atoms, *Science* **325**, 174 (2009).
- [53] F. Zähringer, G. Kirchmair, R. Gerritsma, E. Solano, R. Blatt, and C. F. Roos, Realization of a Quantum Walk with One and Two Trapped Ions, *Phys. Rev. Lett.* **104**, 100503 (2010).
- [54] R. Matjeschk, C. Schneider, M. Enderlein, T. Huber, H. Schmitz, J. Glueckert, and T. Schaetz, Experimental simulation and limitations of quantum walks with trapped ions, *New J. Phys.* **14**, 035012 (2012).
- [55] H. B. Perets, Y. Lahini, F. Pozzi, M. Sorel, R. Morandotti, and Y. Silberberg, Realization of Quantum Walks with Negligible Decoherence in Waveguide Lattices, *Phys. Rev. Lett.* **100**, 170506 (2008).
- [56] A. Crespi, R. Osellame, R. Ramponi, V. Giovannetti, R. Fazio, L. Sansoni, F. De Nicola, F. Sciarrino, and P. Mataloni, Anderson localization of entangled photons in an integrated quantum walk, *Nat. Photonics* **7**, 322 (2013).
- [57] J. B. Spring *et al.*, Boson sampling on a photonic chip, *Science* **339**, 798 (2013).
- [58] M. Tillmann, B. Dakić, R. Heilmann, S. Nolte, A. Szameit, and P. Walther, Experimental boson sampling, *Nat. Photonics* **7**, 540 (2013).
- [59] K. Poullos *et al.*, Quantum Walks of Correlated Photon Pairs in Two-Dimensional Waveguide Arrays, *Phys. Rev. Lett.* **112**, 143604 (2014).
- [60] H. Chalabi, S. Barik, S. Mittal, T. E. Murphy, M. Hafezi, and E. Waks, Synthetic Gauge Field for Two-Dimensional Time-Multiplexed Quantum Random Walks, *Phys. Rev. Lett.* **123**, 150503 (2019).
- [61] M. A. Broome, A. Fedrizzi, S. Rahimi-Keshari, J. Dove, S. Aaronson, T. C. Ralph, and A. G. White, Photonic boson sampling in a tunable circuit, *Science* **339**, 794 (2013).
- [62] A. W. Elshaari, I. E. Zadeh, A. Fognini *et al.*, On-chip single photon filtering and multiplexing in hybrid quantum photonic circuits, *Nat. Commun.* **8**, 379 (2017).
- [63] A. Schreiber, A. Gárbis, P. P. Rohde *et al.*, A 2D quantum walk simulation of two-particle dynamics, *Science* **336**, 55 (2012).

- [64] S. Lepri, C. Trono, and G. Giacomelli, Complex Active Optical Networks as a New Laser Concept, *Phys. Rev. Lett.* **118**, 123901 (2017).
- [65] J. Böhm *et al.*, Microwave Experiments Simulating Quantum Search and Directed Transport in Artificial Graphene, *Phys. Rev. Lett.* **114**, 110501 (2015).
- [66] W. Zhang, K. Cheng, C. Wu, Y. Wang, H. Li, and X. Zhang, Implementing quantum search algorithm with metamaterials, *Adv. Mater.* **30**, 1703986 (2018).
- [67] S. E. Venegas-Andraca, Quantum walks: A comprehensive review, *Quantum Inf. Process.* **11**, 1015 (2012).
- [68] J. Kempe, Quantum random walks: An introductory overview, *Contemp. Phys.* **44**, 307 (2003).
- [69] D. Meyer, From quantum cellular automata to quantum lattice gases, *J. Stat. Phys.* **85**, 551 (1996).
- [70] E. Farhi and S. Gutmann, Quantum computation and decision trees, *Phys. Rev. A* **58**, 915 (1998).
- [71] F. W. Strauch, Connecting the discrete- and continuous-time quantum walks, *Phys. Rev. A* **74**, 030301(R) (2006).
- [72] J. D. Whitfield, C. A. Rodriguez-Rosario, and A. Aspuru-Guzik, Quantum stochastic walks: A generalization of classical random walks and quantum walks, *Phys. Rev. A* **81**, 022323 (2010).
- [73] E. Sánchez-Burillo, J. Duch, J. Gómez-Gardeñes, and D. Zueco, Quantum navigation and ranking in complex networks, *Sci. Rep.* **2**, 605 (2012).
- [74] F. Caruso, Universally optimal noisy quantum walks on complex networks, *New J. Phys.* **16**, 055015 (2014).
- [75] F. M. Andrade, A. G. M. Schmidt, E. Vicentini, B. K. Cheng, and M. G. E. da Luz, Green's function approach for quantum graphs: An overview, *Phys. Rep.* **647**, 1 (2016).
- [76] F. M. Andrade and S. Severini, Unitary equivalence between the Green's function and Schrödinger approaches for quantum graphs, *Phys. Rev. A* **98**, 062107 (2018).
- [77] M. Newman, *Networks: An Introduction* (Oxford University Press, New York, 2010).
- [78] E. Estrada, *The Structure of Complex Networks* (Oxford University Press, New York, 2011).
- [79] M. Barthélemy, Spatial networks, *Phys. Rep.* **499**, 1 (2011).
- [80] A.-L. Barabási and R. Albert, Emergence of scaling in random networks, *Science* **286**, 509 (1999).
- [81] M. Galiceanu, Relaxation dynamics of scale-free polymer networks, *Phys. Rev. E* **86**, 041803 (2012).
- [82] A. Jurjiu, D. Gomes Maia, Jr., and M. Galiceanu, Relaxation dynamics of generalized scale-free polymer networks, *Sci. Rep.* **8**, 3731 (2018).
- [83] O. Mülken and A. Blumen, Continuous-time quantum walks: Models for coherent transport on complex networks, *Phys. Rep.* **502**, 37 (2011).
- [84] X. P. Xu, Exact analytical results for quantum walks on star graphs, *J. Phys. A: Math. Theor.* **42**, 115205 (2009).
- [85] M. Galiceanu and W. T. Strunz, Continuous-time quantum walks on multilayer dendrimer networks, *Phys. Rev. E* **94**, 022307 (2016).
- [86] C. M. Maciel, W. T. Strunz, and M. Galiceanu, Quantum transport on modified multilayered spiderwebs, *J. Phys. A: Math. Theor.* **51**, 495301 (2018).
- [87] P. Reberntrost, M. Mohseni, I. Kassal, S. Lloyd, and A. Aspuru-Guzik, Environment-assisted quantum transport, *New J. Phys.* **11**, 033003 (2009).
- [88] C. Benedetti, M. A. C. Rossi, and M. G. A. Paris, Continuous-time quantum walks on dynamical percolation graphs, *Europhys. Lett.* **124**, 60001 (2018).
- [89] N. Kulvelis, M. Dolgushev, and O. Mülken, Universality at Breakdown of Quantum Transport on Complex Networks, *Phys. Rev. Lett.* **115**, 120602 (2015).
- [90] O. Mülken, M. Dolgushev, and M. Galiceanu, Complex quantum networks: From universal breakdown to optimal transport, *Phys. Rev. E* **93**, 022304 (2016).
- [91] L. K. Gallos and P. Argyrakis, Absence of Kinetic Effects in Reaction-Diffusion Processes in Scale-Free Networks, *Phys. Rev. Lett.* **92**, 138301 (2004).
- [92] S. N. Dorogovtsev and J. F. F. Mendes, Evolution of networks with aging of sites, *Phys. Rev. E* **62**, 1842 (2000).
- [93] F. Jasch, C. von Ferber, and A. Blumen, Dynamical scaling behavior of percolation clusters in scale-free networks, *Phys. Rev. E* **70**, 016112 (2004).
- [94] A. N. Samukhin, S. N. Dorogovtsev, and J. F. F. Mendes, Laplacian spectra of, and random walks on, complex networks: Are scale-free architectures really important? *Phys. Rev. E* **77**, 036115 (2008).
- [95] A. Anishchenko, A. Blumen, and O. Mülken, Enhancing the spreading of quantum walks on star graphs by additional bonds, *Quantum Inf. Process.* **11**, 1273 (2012).
- [96] S. Salimi, Continuous-time quantum walks on star graphs, *Ann. Phys. (NY)* **324**, 1183 (2009).